

AutoTaskFormer: Searching Vision Transformers for Multi-task Learning

Yang Liu^{1*}, Shen Yan², Yuge Zhang³, Kan Ren³, Quanlu Zhang³, Zebin Ren^{4*}, Deng Cai¹, Mi Zhang⁵
¹Zhejiang University ²Michigan State University ³Microsoft Research Asia
⁴Vrije Universiteit Amsterdam ⁵The Ohio State University
 lyng_95@zju.edu.cn Quanlu.Zhang@microsoft.com

Abstract

Vision Transformers have shown great performance in single tasks such as classification and segmentation. However, real-world problems are not isolated, which calls for vision transformers that can perform multiple tasks concurrently. Existing multi-task vision transformers are handcrafted and heavily rely on human expertise. In this work, we propose a novel one-shot neural architecture search framework, dubbed AutoTaskFormer (**Automated Multi-Task Vision TransFormer**), to automate this process. AutoTaskFormer not only identifies the weights to share across multiple tasks automatically, but also provides thousands of well-trained vision transformers with a wide range of parameters (e.g., number of heads and network depth) for deployment under various resource constraints. Experiments on both small-scale (2-task Cityscapes and 3-task NYUv2) and large-scale (16-task Taskonomy) datasets show that AutoTaskFormer outperforms state-of-the-art handcrafted vision transformers in multi-task learning. The entire code and models will be open-sourced.

1. Introduction

Vision Transformers have emerged as successful architectures in various domains, including image classification, object detection, and segmentation [10, 20, 31]. However, real-world problems are often interrelated, which necessitates the development of vision transformers capable of performing multiple tasks simultaneously. Autonomous driving is an example that involves multiple tasks including simultaneous lane detection, semantic understanding, obstacle detection, and depth estimation. Multi-task vision transformers leverage shared knowledge among tasks, allow for a reduction of storage and latency during inference, and yield superior performance compared to their single-task counterparts.

Typically, the architectures of such multi-task vision transformers have been handcrafted in the literature [5, 24, 26, 2,

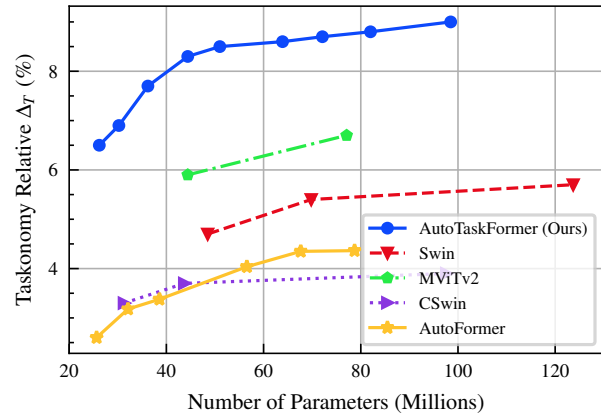


Figure 1. Comparison between AutoTaskFormer and existing transformer-based and NAS-based models on 16-task Taskonomy [37]. We use the relative performance metric Δ_T with respect to the same single-task baseline to compare different models.

34, 35]. For instance, IPT [5] proposes a multi-head multi-tail architecture for four low-level tasks. Mult [2] adopts a shared transformer encoder and six task-specific decoders for high-level dense predictions. InvPT [34] simultaneously models spatial positions and multiple tasks in a unified framework. TaskPrompter [35] designs a set of spatial-channel task prompts and learn their spatial and channel interactions within each transformer layer.

Those handcrafted designs, unfortunately, are limited by two primary constraints. First, manual architecture exploration will likely exceed human design capabilities due to extremely large design spaces. For example, how to choose the best sharing patterns across various tasks and decide the optimal embedding dimensions and the number of heads within each layer. These challenges are magnified as the number of tasks increases. Second, handcraft designs are generally designed for specific multi-task scenarios. Since weight sharing patterns are diverse for different tasks, the multi-task model manually designed for one scenario is hard to generalize to other multi-task scenarios.

Neural architecture search (NAS) has been proposed to

*This work was done during an internship at Microsoft Research Asia

automate the neural architecture design to mitigate manual efforts. Recent NAS advances [6, 4] advocate training one high-quality supernet containing thousands of high-performing subnets that can be directly searched and deployed without extra fine-tuning or re-training. It is natural to ask whether it is possible to obtain a high-quality *multi-task supernet* where every *multi-task subnet* exhibits decent performance. When investigating this problem, we face two major hurdles. First, designing a NAS search space that allows multiple tasks to operate simultaneously while preserving each task’s performance. Second, establishing a process that can automatically configure multi-task networks to fulfill diverse deployment constraints.

In this work, we propose a novel one-shot neural architecture search framework named AutoTaskFormer to tackle these challenges. We construct a sizeable search space based on Swin Transformer [20] that covers the most often-tuned hyper-parameters (*e.g.*, embedding dimension, number of heads) in vision transformers. While this *cell search space* for individual components covers a broad range of networks that can be searched, we determined through empirical observation that it is insufficient for scenarios where the primary challenge is to identify shared patterns among multiple tasks. In order to obtain a high-quality multi-task supernet with properly shared tasks, we advocate sampling multi-task subnets from the same multi-task conditional distribution in both supernet training and search phases. We refer to this multi-task conditional distribution search as *skeleton search* which can be optimized along with the supernet training. To search multi-task subnets under different deployment requirements, we propose a novel criterion to distinguish the good ones from the bad.

Our contributions are: (1) We propose a novel skeleton space integrated with a cell space to simultaneously search task-sharing patterns and detailed network architectures for multi-task learning. (2) We propose a novel one-shot multi-task NAS pipeline that automatically identifies multi-task networks to various deployment requirements without extra fine-tuning. (3) AutoTaskFormer achieves state-of-the-art multi-task learning performance on both small-scale (2-task Cityscape [8] and 3-task NYUv2 [27]) and large-scale (16-task Taskonomy [37] (shown in Fig.1)) datasets, and can be easily adapted to new domains and tasks yielding better generalization than handcrafted transformers.

2. Related Work

Vision Transformers. Our work is related to vision transformers. ViT [10] proposes the first design for image classification task by stacking transformer blocks on linear projections of non-overlapping image patches. Swin Transformer [20] introduces non-overlapping window partitions and restricts self-attention within each window. MViTv2 [17] incorporates decomposed relative positional embeddings and

residual pooling connections to obtain a feature hierarchy from multiple stages. These works focus on designing general backbone networks that need human expertise to design task decoders when adapted to downstream tasks. In contrast, AutoTaskFormer is a framework that automates multi-task vision transformer design.

Neural Architecture Search (NAS). Our work is also related to NAS [36, 6, 7]. Most recent efforts in NAS focus on one-shot weight-sharing strategy to amortize search cost [30, 15, 3]. The key idea is to train an over-parameterized supernet and share the weights among subnets [36, 15]. However, most existing NAS studies focus on searching network architectures for a single task. As we will explain in the next section, directly extending the one-shot weight-sharing strategy from single-task NAS to multi-task NAS incurs interferences among tasks, leading to significant performance degradation. AutoTaskFormer tackles this problem using a novel NAS pipeline that involves two search stages instead of one, specifically designed for multi-task learning.

Multi-task Learning (MTL). MTL aims to learn parameter sharing across multiple tasks. For example, Cross-Stitch [23] manually employs an additional group of shared units to merge multiple task backbones. Sluice [25] jointly learns a latent multi-task architecture and task-specific models. NDDR-CNN [13] proposes a novel CNN structure to learn a discriminative feature embedding for each task. There are several works that design task-sharing architectures through NAS. In particular, MTL-NAS [12] starts with two task-specific networks and seeks optimal edges between the inter-task branches. AdaShare [29] learns the sharing weights through a task-specific policy that selectively chooses which layers to execute for a given task. AutoMTL [38] proposes a source-to-source compiler that transforms the backbone CNN into a supermodel. However, due to the bottom-up approach of combining task-specific networks, the sharing between tasks and networks needs to be meticulously designed and hence can only support a small number of tasks. In contrast, AutoTaskFormer adopts a top-down approach that supports many more tasks with a novel NAS pipeline.

3. AutoTaskFormer

3.1. From Single-task NAS to Multi-task NAS

To search a descent architecture within a vast space, a weight-sharing strategy is commonly leveraged to avoid exhausted subnet training from scratch [36, 6, 7]. For a supernet \mathcal{A} with weights \mathcal{W} , each subnet α directly inherits its weights $\mathcal{W}_{\mathcal{A}}(\alpha)$ from \mathcal{W} . The one-shot NAS is thus formulated as a two-stage optimization problem, *i.e.*, supernet training and architecture searching.

During supernet training, one or several subnets are sampled from \mathcal{A} to directly update supernet weights \mathcal{W} [6, 7] (as shown in Fig. 2(a)). By sharing weights among various sub-

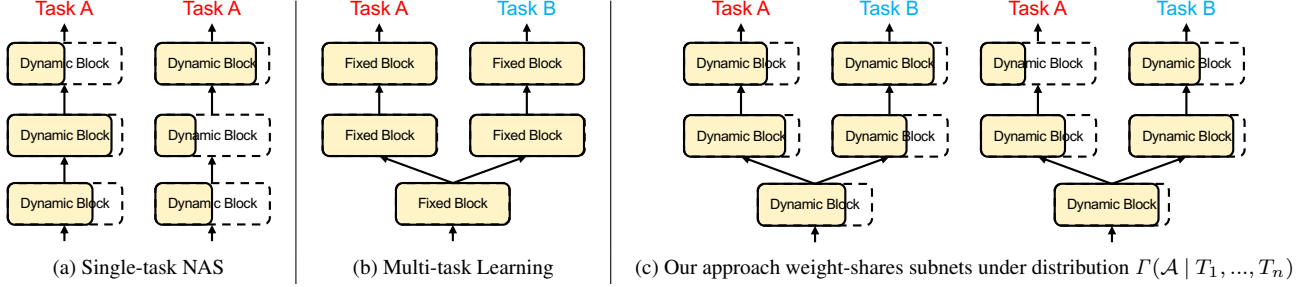


Figure 2. (a) Single-task NAS shares weights among various subnets in supernet training where subnets are sampled according to prior (uniform) distribution $\Gamma(\mathcal{A})$. (b) Multi-task learning shares part of the network weights for common knowledge. (c) Our approach encourages weight-sharing among multi-task subnets that are sampled from task conditional distribution $\Gamma(\mathcal{A} | T_1, \dots, T_n)$.

nets with weights inherited from \mathcal{W} , two-stage NAS makes every subnet $\alpha \in \mathcal{A}$ sufficiently trained such that they can be directly used for deployment without extra fine-tuning. To summarize, single-task NAS shares weights among various subnets during supernet training that minimize:

$$\mathcal{W}^* = \operatorname{argmin}_{\mathcal{W}} \mathbb{E}_{\alpha \sim \Gamma(\mathcal{A})} [\mathcal{L}(\mathcal{W}_{\mathcal{A}}(\alpha))], \quad (1)$$

where $\Gamma(\mathcal{A})$ is a prior distribution of $\alpha \in \mathcal{A}$ and is empirically instantiated by uniform sampling [15].

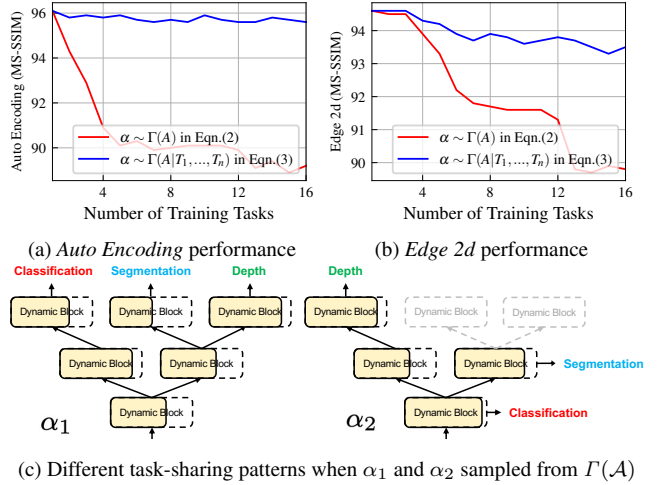
In comparison, **for multi-task NAS where α denotes multi-task subnet and \mathcal{A} is its supernet** (see example multi-task subnets in Fig. 2(c)), a straightforward idea is to extend the single-task objective to a sum of multiple losses:

$$\mathcal{W}^* = \operatorname{argmin}_{\mathcal{W}} \mathbb{E}_{\alpha \sim \Gamma(\mathcal{A})} \left[\sum_{i=1}^n \lambda_i \mathcal{L}_i(\mathcal{W}_{\mathcal{A}}(\alpha)) \right], \quad (2)$$

where λ_i and \mathcal{L}_i are the pre-defined task weight and loss metric for the i -th task, respectively. An early experiment, shown in Fig. 3(a-b), shows that this simple extension has huge interference among different tasks.

Digging for deeper reasons why Eqn. (2) does not work well for multi-task NAS, we found that weight-sharing is also widely used in previous multi-task (without NAS) literature. However, their weight-sharing paradigm is quite different from NAS. As shown in Fig. 2(b), Instead of sharing weights among multiple candidate subnets in NAS, they share part of network blocks (e.g., the early stage of backbones) across different tasks. If properly shared, it can effectively avoid negative knowledge transfer [29, 14]. It is also shown in the literature [28] that if the sharing is done erroneously (e.g., sharing among irrelevant tasks), multi-task learning will produce results even worse than single-task learning.

Since the weight-sharing among multiple tasks is not explicitly considered in Eqn. (2), when supernet training, both proper and erroneous multi-task subnets might be sampled. We illustrate with a simple example in Fig. 3(c). Assuming α_2 here is a low-quality subnet (e.g., predicting highly



(a) Auto Encoding performance (b) Edge 2d performance (c) Different task-sharing patterns when α_1 and α_2 sampled from $\Gamma(\mathcal{A})$

Figure 3. (a-b): Two sharing strategies in supernet training for tasks *Auto Encoding* and *Edge 2d* (from Taskonomy[37]) respectively when the number of trained tasks increase. (c): Example two 3-task subnets α_1, α_2 sampled from the uniform distribution $\Gamma(\mathcal{A})$.

semantic classification with low-level features) that fails to converge, it will disturb the training of α_1 due to the subnets' weight-sharing in NAS, thus ruining the whole training. To obtain a high-quality supernet for multi-task NAS, it is crucial to ensure that all subnets are qualified. In other words, *we need a search space for multi-task supernet that we can sample well-qualified subnets under the same task-sharing pattern*. This is expressed as

$$\mathcal{W}^* = \operatorname{argmin}_{\mathcal{W}} \mathbb{E}_{\alpha \sim \Gamma(\mathcal{A} | T_1, \dots, T_n)} \left[\sum_{i=1}^n \lambda_i \mathcal{L}_i(\mathcal{W}_{\mathcal{A}}(\alpha)) \right], \quad (3)$$

where $\Gamma(\mathcal{A} | T_1, \dots, T_n)$ is a conditional distribution of $\alpha \in \mathcal{A}$ with respect to task T_1, \dots, T_n .

In the rest of this section, we first review the background of vision transformers. We then introduce how to get $\Gamma(\mathcal{A} | T_1, \dots, T_n)$, which we refer to as skeleton search. Finally, we elaborate our whole pipeline for multi-task NAS.

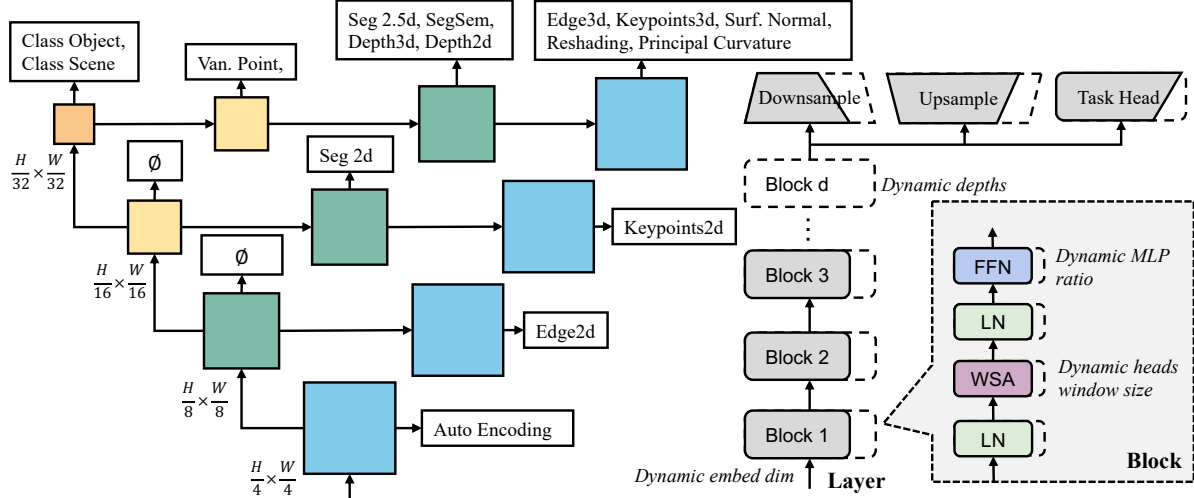


Figure 4. **Left:** The skeleton space of AutoTaskFormer supernet where tasks can be attached at any adhoc point of middle layers. We show an example of searched vision transformer where \emptyset indicates no task is attached at that layer. **Right:** The cell space where we search the optimal embedding dimension and depths for each layer, the number of heads, MLP ratio, and window size for each transformer block.

3.2. Encoder-Decoder based Vision Transformer

We review the encoder-decoder structure with window attention [20], which serves as a basis of AutoTaskFormer.

During encoding, a 2D image is first transformed into patch embeddings by linear projection and then fed into the transformer layers. Fig. 4 (Right) shows that a transformer layer consists of alternating blocks of window-partitioned multi-head self-attention (WSA) and feed-forward network (FFN). Layer normalization (LN) is applied before and after the residual connection of every block.

During decoding, an upsampling layer is attached before each transformer layer to double the spatial resolution and halve the channel dimension. The decoder exploits semantic information at different stride levels and gradually recovers information in a coarse-to-fine manner.

3.3. Search Space

(Macro) Skeleton search space. Our AutoTaskFormer is constructed on the basis of the encoder-decoder Swin Transformer, as illustrated in Fig. 4 (Left). We extend the encoder by appending additional decoding layers at the middle levels. This architectural alteration introduces minimal parameters, as the majority of the parameters are concentrated at layers of size 1/16 and 1/32 [20]. The branched transformer design increases the search space by generating multiple multiscale features from different levels of the encoder.

We define a **skeleton** to be a single acyclic path. Fig. 5 illustrates that the skeleton can either be single-scale, generating a single feature map for downstream tasks, or multi-scale, producing a feature hierarchy of sizes 1/4, 1/8, 1/16, and 1/32. For example, the single-scale skeleton space, depicted

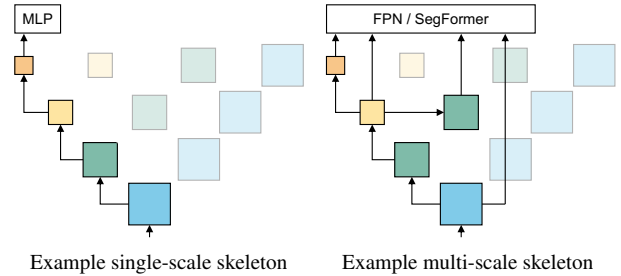


Figure 5. **Left:** Single-scale skeletons cover existing designs like Swin [20]. **Right:** Multi-scale skeletons produce a multi-scale feature hierarchy for FPN [18] or SegFormer [33].

in Fig. 5 (Left), includes the decoder-free Swin [20]. On the other hand, the multi-scale skeleton space, shown in Fig. 5 (Right), is versatile enough to cater to multi-scale task heads, such as FPN [18] and SegFormer [33].

The skeleton space (either single-scale or multi-scale) is pre-defined by users according to their requests. In Fig. 4 (Left), we show that AutoTaskFormer has $\{\text{orange} \times 1, \text{yellow} \times 2, \text{green} \times 3, \text{blue} \times 4\}$ transformer layers to obtain a feature hierarchy of size 1/32, 1/16, 1/8, and 1/4, respectively. We allow output features from any transformer layers for single-scale skeleton, resulting in $10 = C_{4+3+2+1}^1$ searchable skeletons for each task. For multi-scale, we allow features from any combination of transformer layers with different resolutions, resulting in $24 = C_4^1 C_3^1 C_2^1 C_1^1$ candidates for each task.

Though the number of candidate skeletons for each task is limited, the skeleton space will exponentially increase according to the number of training tasks. For example, in 16 tasks learning, it contains 10^{16} and 24^{16} candidate skeletons in single-scale and multi-scale space, respectively.

(Micro) Cell search space. We define a **cell** to be a single transformer layer consisting of a dynamic number of transformer blocks. As shown in Fig. 4 (Right), each block follows the design of the Swin Transformer but with a searchable number of heads, MLP ratio, and window size. Since the input and output of a transformer block are connected via a shortcut connection, the embedding dimensions of input and output tensors should be consistent across all transformer blocks within the same cell. Thus, embedding dimension and depths are the cell-wise searchable parameters, while window size, number of heads, and MLP ratio are the block-wise searchable parameters.

Following the weight sharing paradigm [6], we encode the cell search space into a supernet. Every model in the search space is a subnet of the supernet, and all subnets share weights of their common parts. The supernet is the largest model in that space that owns the largest number of transformer blocks, the number of heads, embedding dimension, and MLP ratio within each transformer layer. According to the constraints on model parameters, we partition the cell space following the designs of Swin-S and Swin-B. The detailed cell search space is described in Appendix B.4.

3.4. Search Algorithm and Multi-task NAS Pipeline

Skeleton search algorithm. We propose to simultaneously search skeletons for each task in multi-task supernet training such that tasks will share certain stages of knowledge according to their favored skeletons. The skeleton search algorithm is detailed as follows:

For the s -th skeleton in skeleton space \mathbf{S} , we seek a binary variable $u_{s,k}$ to determine whether that skeleton is searched to execute the k -th task $T_k \in \mathbf{T}$, yielding the best overall performance for all tasks. The selection among all candidate skeletons for all tasks is denoted by $\mathbf{U} = \{u_{s,k}\}$, where each column is a one-hot vector.

To jointly optimize \mathbf{U} along with network parameters through back-propagation, we adopt the Gumbel-softmax trick [16]. Concretely, We let $\pi_k \in \mathbb{R}^{|\mathbf{S}|}$ be the distribution vector of the k -th column of \mathbf{U} that we want to optimize, where the $\pi_{k,s}$ represents the probability that the s -th skeleton is selected to execute in the k -th task. We relax column-wise one-hot \mathbf{U} to soft $\mathbf{U}' = \{u'_{s,k}\}$ by the reparameterization trick [16]:

$$u'_{s,k} = \frac{\exp((\log \pi_{k,s} + \epsilon_s)/\tau)}{\sum_{s' \in \mathbf{S}} \exp((\log \pi_{k,s'} + \epsilon_{s'})/\tau)}, \quad (4)$$

where $\epsilon \in \mathbb{R}^{|\mathbf{S}|}$ is a vector with i.i.d. samples drawn from Gumbel distribution (0, 1), and τ is the softmax temperature. We initialize $\tau = 5$ and gradually anneal it down to 0 during training. For inference, we discretize \mathbf{U}' to get \mathbf{U} by argmax, which is the preferred skeleton of each task.

Multi-task NAS pipeline. Our multi-task NAS also includes train and search stages like conventional single-task NAS [36, 6, 7]. We detail the multi-task NAS pipeline as follows (see pseudo-codes in Appendix A):

Train Stage: Multi-task Supernet Training. In each iteration, we uniformly sample the largest, the smallest, and two middle-sized subnets from the cell space. For each sampled subnet, we calculate all task losses from all candidate skeletons in a loss matrix $\mathcal{L} \in \mathbb{R}^{|\mathbf{S}| \times |\mathbf{T}|}$, where $|\cdot|$ indicates the cardinality of the set. We use \mathbf{U}' in Eqn. (4) to weighted accumulate losses with respect to all candidate skeletons for each task, and the final loss l is defined as:

$$l = \sum_k \sum_s \lambda_k u'_{s,k} * \mathcal{L}_{s,k}, \quad (5)$$

where λ_k is the pre-defined weight for the k -th task included in Appendix B. We use l to update both supernet parameters and skeleton distributions \mathbf{U}' .

Search Stage 1: Skeleton Space Search. We perform the skeleton search before the cell space search to obtain optimal network structures for \mathbf{T} tasks. Specifically, we first obtain discrete \mathbf{U} from \mathbf{U}' by argmax to decide the favored skeleton for each task. Then, we union the skeletons for all tasks in \mathbf{T} to find the least common parts of layers, such that we can perform those tasks concurrently. Let's take two skeletons (2-task) as an example: b1->head1 for task T_1 and b1->pool1->b2->head2 for task T_2 . We break down each skeleton into a set of components (e.g., T_1 consists of {b1, head1}). Afterward, we take the union of these two sets to obtain the multi-task (2-task) architecture.

Search Stage 2: Cell Space Search. To enable searches among thousands of subnets in \mathcal{A} to perform \mathbf{T} tasks concurrently, we first define a criterion to distinguish good multi-task subnets from bad ones. Motivated by [22, 29], for subnet $\alpha \in \mathcal{A}$ on task $T_k \in \mathbf{T}$, we use $\gamma(T_k; \alpha)$ to represent the relative multi-task performance for subnet α with respect to the averaged performances by:

$$\gamma(T_k; \alpha) = \frac{1}{|M|} \sum_{j=0}^{|M|} (-1)^{m_j} \frac{M_{\alpha,j} - \frac{1}{|\mathcal{A}|} \sum_{\alpha'} M_{\alpha',j}}{\frac{1}{|\mathcal{A}|} \sum_{\alpha'} M_{\alpha',j}}, \quad (6)$$

where $|M|$ is the number of metrics of the task T_k and m_j is 1 if a lower value represents a better performance for j -th metric and 0 otherwise. $M_{\alpha,j}$ is the value of j -th metric in task T_k for subnet α . We then define $\gamma(\alpha)$ to be the average relative performance for subnet α :

$$\gamma(\alpha) = \frac{1}{|\mathbf{T}|} \sum_{T_k \in \mathbf{T}} \gamma(T_k; \alpha). \quad (7)$$

We search for subnets $\alpha \in \mathcal{A}$ according to $\gamma(\alpha)$ that yield the best multi-task performance under different resource constraints via the evolution search [6, 15] in Appendix B.5.

Models	#Params	Point Predictions			Dense Predictions														$\Delta_T \uparrow$
		Acc. \uparrow		Loss \downarrow	mIoU \uparrow		MS-SSIM \uparrow										Loss \downarrow		
		Obj.	Scene	Van. Pt	SegSem	D_e	D_z	$E2d$	$E3d$	$\mathcal{K}2d$	$\mathcal{K}3d$	\mathcal{N}	PC	\mathcal{R}	AE	Seg2d	Seg2.5d		
Swin-T	48.5	52.4	63.5	1.376	41.3	87.8	87.8	89.7	73.1	91.4	55.5	71.6	66.2	68.7	95.1	0.368	0.129	4.7	
CSwin-T	31.3	52.0	63.8	1.388	39.6	88.0	88.0	88.7	72.6	91.5	55.0	71.1	66.0	69.0	94.6	0.407	0.133	3.3	
MViTv2-T	44.3	53.3	66.3	1.346	45.5	88.2	88.2	87.7	73.2	90.6	56.1	71.8	66.3	70.0	93.9	0.381	0.128	5.9	
AutoFormer	38.6	51.9	63.8	1.608	36.2	87.9	87.9	92.6	73.8	93.9	55.8	72.6	66.4	70.6	94.1	0.362	0.130	3.4	
AutoTaskFormer (Ours)	45.5	53.8	66.5	1.367	45.6	88.6	88.6	93.9	75.8	95.4	59.0	75.3	67.6	73.2	95.8	0.358	0.127	8.4	
Swin-S	69.8	53.3	65.4	1.492	43.2	88.1	88.1	89.9	73.7	91.7	56.6	72.4	66.6	70.1	95.2	0.368	0.128	5.4	
CSwin-S	43.7	51.9	64.5	1.630	40.6	88.3	88.3	93.5	74.7	94.3	57.2	73.9	66.9	72.3	88.6	0.430	0.129	3.7	
MViTv2-S	55.0	53.5	66.3	1.461	45.4	88.3	88.3	88.6	73.7	91.3	56.9	72.3	66.5	70.7	94.3	0.395	0.130	5.6	
AutoFormer	56.6	52.3	64.4	1.584	38.3	87.9	87.9	93.4	74.3	94.7	56.6	73.0	66.6	71.1	94.6	0.377	0.129	4.2	
AutoTaskFormer (Ours)	52.2	54.0	66.8	1.353	45.9	88.5	88.5	94.0	76.0	96.0	59.1	75.5	67.7	73.4	95.8	0.349	0.126	8.9	
Swin-B	107.7	53.4	65.0	1.397	42.7	88.1	88.2	90.6	74.0	92.5	56.7	72.7	66.6	70.3	95.4	0.375	0.129	5.7	
CSwin-B	97.6	52.6	66.0	1.639	42.0	87.8	87.8	94.1	75.2	95.4	58.2	74.5	67.0	72.7	91.0	0.483	0.129	3.9	
MViTv2-B	71.5	54.0	67.3	1.447	46.6	88.5	88.5	88.3	74.0	91.1	57.3	72.8	66.7	71.2	94.1	0.369	0.126	6.7	
AutoFormer	67.6	52.5	64.7	1.616	39.2	87.9	87.9	93.5	74.5	94.8	57.1	73.3	66.8	71.4	94.6	0.383	0.130	4.4	
AutoTaskFormer (Ours)	65.1	54.2	67.0	1.350	47.2	88.7	88.7	93.8	76.4	95.9	59.8	75.9	67.9	73.9	95.9	0.353	0.125	9.4	

Table 1. Comparisons of 16-task learning on Taskonomy with both transformer-based and NAS-based models. Van. Pt’s l_2 loss is multiplied by a factor of 100 for better readability. The highest performance is marked in **bold** in each category.

4. Experiments

4.1. AutoTaskFormer for Taskonomy

Tasks. To conduct a comprehensive evaluation, we incorporated 11 additional tasks from the original Taskonomy dataset [37], beyond the 5 dense prediction tasks assessed in previous works [29, 38]. This extension allows us to cover a wider range of task types that include **3 point prediction tasks**: object classification (Obj.), scene classification (Scene), and vanishing point regression (Van. Pt), as well as **13 dense prediction tasks**: depth euclidean (D_e), depth zbuffer (D_z), edge texture ($E2d$), edge occlusion ($E3d$), 2D keypoint detection ($\mathcal{K}2d$), 3D keypoint detection ($\mathcal{K}3d$), surface normal (\mathcal{N}), principal curvatures (PC), reshading (\mathcal{R}), auto encoding (AE), unsupervised 2d segmentation (Seg2d), unsupervised 2.5d segmentation (Seg2.5d), and semantic segmentation (SegSem).

Metrics and Baselines. We use top-1 accuracy for classifications, mIoU for semantic segmentation, and MS-SSIM [32] for other dense tasks. For unsupervised Seg2d, Seg2.5d and Van. Pt, we report their absolute losses. To compare the overall multi-task performance for different models, we use relative performance Δ_T [22] with respect to the single task baseline (Swin-T for Taskonomy). The calculation of Δ_T is equivalent to Eqn. (6) except for replacing averaged subnets performance with single-task baseline performance. We use single-scale transformers followed by standard FCN [21] heads for all dense predictions. For point predictions, we use global average pooling followed by a simple MLP.

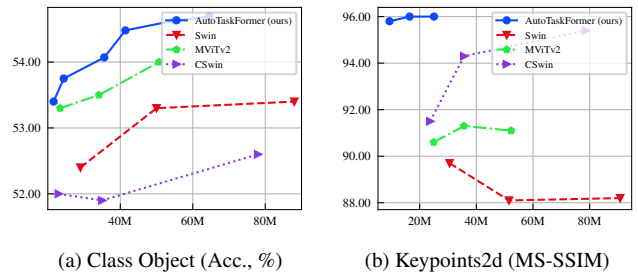


Figure 6. Performance of single-task models after multi-task training on Taskonomy. The other 14 tasks’ models are in Appendix Fig.10.

Results. Tab. 1 shows that our AutoTaskFormers are consistently better than the baseline Swin Transformer [20] by 3.5~3.7% on multi-task performances. AutoTaskFormer outperforms the state-of-the-art transformer models CSwin [9] and MViTv2 [17] by 2.5%~3.6%. Regarding the absolute task performances, AutoTaskFormer surpasses baseline Swin and the latest MViTv2 in nearly all the tasks, illustrating the impact of multi-task NAS in designing and exploring architectures.

We compare the flexibility of NAS with other handcrafted vision transformers through the evaluation of our single-task subnet. As illustrated in Fig. 6, the parameter range of our single-task subnet varies based on the tasks and their preferred skeletons. Thus we can directly sample a $\sim 5M$ parameter transformers (roughly three-quarters smaller than other handcrafted transformers) to perform 2D keypoint estimation without extra fine-tuning.

Model Type	Models	#Params (M)	Semantic Seg.		Depth Prediction				
			mIoU \uparrow	PAcc \uparrow	Error \downarrow		δ within \uparrow		
					Abs	Rel	1.25	1.25 ²	1.25 ³
CNN (non-NAS MTL models)	Cross-Stitch [23]	42.6	40.3	74.3	0.017	0.34	70.0	86.3	93.1
	Sluice [25]	42.6	39.8	74.2	0.018	0.35	68.9	85.8	92.8
	NDDR-CNN [13]	44.6	41.5	74.2	0.018	0.35	69.9	86.3	93.0
CNN (NAS MTL models)	DEN [1]	23.8	38.0	74.2	0.017	0.37	72.3	87.1	93.4
	Adashare [29]	21.3	41.5	74.9	0.016	0.33	75.5	89.9	94.9
	AutoMTL [38]	28.8	42.8	74.8	0.018	0.33	70.0	86.6	93.4
Transformer (single-scale)	Swin [20]	30.6	49.4	91.3	0.015	0.28	76.2	90.3	95.4
	CSwin [9]	23.2	46.1	90.6	0.015	0.29	75.8	90.0	95.3
	MViTv2 [17]	26.4	52.2	91.8	0.015	0.27	76.7	90.7	95.7
	AutoTaskFormer (ours)	26.3	54.7	92.2	0.013	0.27	77.7	91.3	96.0
Transformer (multi-scale)	Swin [20]	28.8	51.3	91.5	0.017	0.30	74.6	89.2	95.0
	CSwin [9]	22.8	50.7	91.5	0.016	0.30	75.5	89.8	95.2
	MViTv2 [17]	24.6	55.1	92.5	0.015	0.27	76.4	90.6	95.9
	AutoTaskFormer (ours)	27.0	56.8	92.8	0.012	0.27	78.8	91.7	96.1

Table 2. Comparison of 2-task learning on Cityscapes with both CNN-based and transformer-based methods. We use the tiny version of all baseline transformers to obtain similar parameters in CNN methods. The multi-scale transformer uses SegFormer task head [33].

Models	#Params (M)	SemSeg.		Surface Normal				Depth MS-SSIM \uparrow
		mIoU \uparrow	PAcc \uparrow	$\Delta\theta$ \downarrow	$\Delta\theta$, within (%) \uparrow			
					11.25 $^\circ$	22.5 $^\circ$	30 $^\circ$	
Swin-S	53.5	30.3	62.0	11.3	63.9	86.5	92.9	85.0
CSwin-S	36.2	27.1	59.5	11.0	65.6	86.8	92.8	86.7
MViTv2-S	38.6	32.7	63.7	10.9	65.5	87.0	93.1	87.1
AutoTaskFormer	35.3	33.2	64.4	10.0	69.4	88.3	93.7	88.0

Table 3. Comparison of 3-task transfer learning on NYUv2 with other transformer-based models. All models are first pre-trained on Taskonomy and then fine-tuned on NYUv2.

Models	Jigsaw	Inpaint	Denoise
	Acc. \uparrow	MS-SSIM \uparrow	MS-SSIM \uparrow
Swin-S	66.2	67.1	86.3
CSwin-S	50.7	69.4	87.9
MViTv2-S	64.4	73.1	92.3
AutoTaskFormer	72.0	73.2	93.0

Table 4. Comparison of 3-task generalization on Taskonomy with other transformer-based models. All models are pre-trained by 16 tasks on Taskonomy, with the frozen backbone, and new task heads attached for generalization.

4.2. AutoTaskFormer for Cityscapes

Cityscapes [8] consists of high-resolution street-view images. We use this dataset for semantic segmentation and depth estimation tasks following [19]. We evaluate both mIoU and pixel accuracy (PAcc) for segmentation. For depth estimation, we compute both absolute errors and the relative difference between the prediction and ground truth via the percentage of $\delta = \max\{\frac{y_{pred}}{y_{gt}}, \frac{y_{gt}}{y_{pred}}\}$ following [11].

We evaluate performances for both single-scale skeletons with MLP task heads and multi-scale skeletons with SegFormer [33] heads. Tab. 2 shows that AutoTaskFormer outperforms baseline Swin Transformer by a large margin of $\sim 4\%$ on semantic segmentation for both single-scale and multi-scale downstream task heads. Furthermore, it surpasses the most modern CSwin and MViTv2.

4.3. Transfer Learning

Generalize to new domains. NYUv2 [27] comprises 1449 images from 464 different indoor scenes providing

similar depth estimation, surface normal and semantic segmentation as in Taskonomy. We follow [13] to evaluate multiple metrics for this dataset. Due to the scarcity of examples to train the vision transformer, we use this dataset to evaluate the transferability (*i.e.*, attached new task heads and fine-tune the backbone models) to the unseen domain. Tab. 3 shows that AutoTaskFormer yields better generalization when adapted to similar tasks under new domains.

Generalize to new tasks. We also show how well AutoTaskFormer generalizes to new tasks on Taskonomy without fine-tuning the backbone. The transferred tasks include jigsaw puzzle, denoising, and image inpainting from [37]. In contrast to other training tasks in Sec. 4.1, the novel tasks own completely different input styles (*i.e.*, gaussian blurred, random puzzle permuted, or corrupted) and is thus challenging if we freeze the backbone network. The results in Tab. 4 show that AutoTaskFormer has better generalization performance when adapted to novel tasks under the same domain.

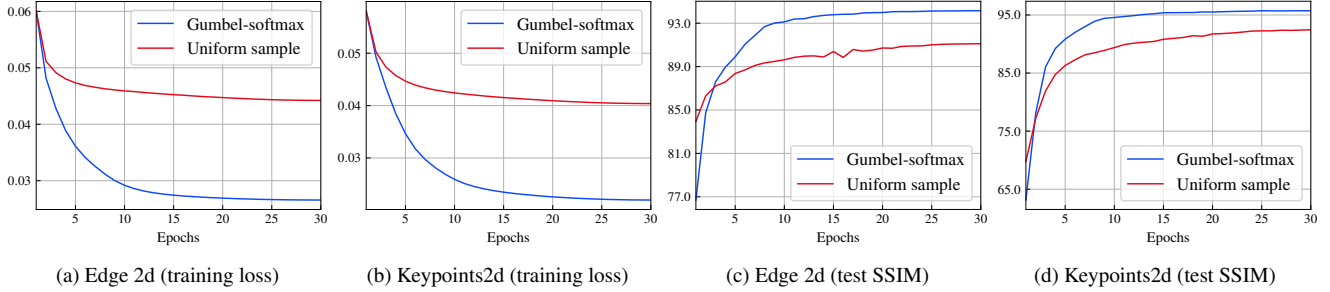


Figure 7. Comparison between using and not using Gumbel-softmax to search task-favored skeletons in AutoTaskFormer: **(a-b)** compare the training loss between Gumbel-softmax and uniform sampling; **(c-d)** compare the validation performance during supernet training.

AutoTaskFormer			#params (M)	Δ_T (%)
Skeleton space	Skeleton search	Cell space		
✗	✗	✗	41.0	4.4
✓	✗	✗	43.5	6.3
✓	✓	✗	43.5	7.1
✓	✓	✓	22.3 – 108.7	7.0 – 9.4

Table 5. Ablation studies of AutoTaskFormer on Taskonomy.

4.4. Ablation Studies

Skeleton space vs. SwinUNET. As shown in Fig. 5 (b), the largest skeleton in our single-scale framework is almost identical to SwinUNET (the baseline model in Tab. 5). As discussed in Sec. 3.1 and shown in Fig. 3, directly applying weight sharing as to joint train multi-task supernet is inappropriate. In contrast, AutoTaskFormer benefits from the tree structures that branched out at different levels of the encoder. We show quantitative results in Tab. 5 that our single-scale skeleton space provides $\sim 2\%$ relative improvements on Taskonomy. On the other hand, our multi-scale skeleton space is about three times larger than SwinUNET that provides more optional skeletons for downstream multi-scale task heads like FPN [39] and SegFormer [33].

Gumbel-softmax skeleton search. AutoTaskFormer uses Gumbel-softmax [16, 29] to search the favored skeletons for each task during training and directly uses the searched skeleton for each task during the test. Another option is to uniformly sample skeletons during training and then search the task-favored skeleton according to its validation performance. In Fig. 7, we compare these two methods on training loss and validation accuracy. It can be observed that the task training loss would be easily saturated at an early stage when we uniformly sample skeletons during training. A possible reason is that it would be impractical to expect less informative skeletons (e.g., a skeleton with a single transformer layer) to perform highly semantic predictions.

In contrast, AutoTaskFormer uses Gumbel-softmax to search the favored skeleton for each task as presented in Sec. 3.4. Theoretically, there exists a negative correlation between

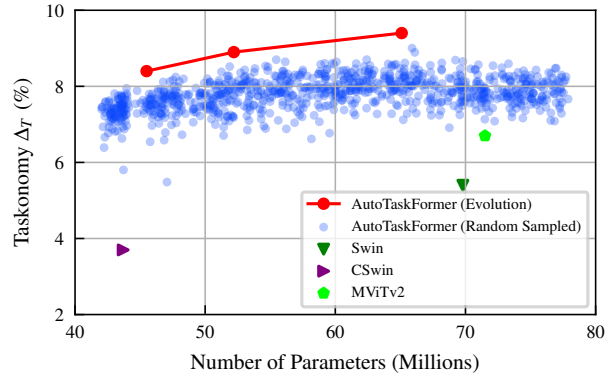


Figure 8. Taskonomy performance of AutoTaskFormer and 1000 randomly sampled subnets within 40-80M parameters.

$w'_{s,k}$ and $\mathcal{L}_{s,k}$ in Eqn. (5) when minimizing the overall loss l . It indicates that the k -th task gradually prefers the s -th skeleton with the minimum objective loss $\mathcal{L}_{s,k}$ and ignores the other candidate skeletons to prevent saturation. Fig. 7 (c-d) show that Gumbel-softmax search brought significant improvements for tasks like *edge2d* and *keypoints2d*.

Cell search space. AutoTaskFormer adopts one-shot supernet training for multi-task NAS by weight sharing [6]. The blue points in Fig. 8 show that there a large number of subnets achieving good performance when inheriting weights from the supernets. By adopting evolution search, AutoTaskFormer consistently achieves $\sim 0.5\%$ higher performances than the random search.

5. Conclusion

In this work, we present AutoTaskFormer, a novel one-shot neural architecture search framework for multi-task vision transformers. AutoTaskFormer not only identifies the optimal skeleton for each task automatically but also adapts the cell designs in vision transformers to various resource constraints. AutoTaskFormer outperforms existing methods on multi-task benchmarks and exhibits promising generalization capabilities to unseen tasks and domains.

References

- [1] Chanho Ahn, Eunwoo Kim, and Songhwai Oh. Deep elastic networks with model selection for multi-task learning. In *Proceedings of the IEEE/CVF international conference on computer vision*, pages 6529–6538, 2019. 7
- [2] Deblina Bhattacharjee, Tong Zhang, Sabine Süsstrunk, and Mathieu Salzmann. Mult: An end-to-end multitask learning transformer. In *Proceedings of the IEEE/CVF Conference on Computer Vision and Pattern Recognition*, pages 12031–12041, 2022. 1
- [3] Andrew Brock, Theo Lim, JM Ritchie, and Nick Weston. Smash: One-shot model architecture search through hypernetworks. In *International Conference on Learning Representations*, 2018. 2
- [4] Han Cai, Chuang Gan, Tianzhe Wang, Zhekai Zhang, and Song Han. Once for all: Train one network and specialize it for efficient deployment. In *International Conference on Learning Representations*, 2020. 2
- [5] Hanting Chen, Yunhe Wang, Tianyu Guo, Chang Xu, Yiping Deng, Zhenhua Liu, Siwei Ma, Chunjing Xu, Chao Xu, and Wen Gao. Pre-trained image processing transformer. In *Proceedings of the IEEE/CVF Conference on Computer Vision and Pattern Recognition*, pages 12299–12310, 2021. 1
- [6] Minghao Chen, Houwen Peng, Jianlong Fu, and Haibin Ling. Autoformer: Searching transformers for visual recognition. In *Proceedings of the IEEE/CVF International Conference on Computer Vision*, pages 12270–12280, 2021. 2, 5, 8, 11
- [7] Minghao Chen, Kan Wu, Bolin Ni, Houwen Peng, Bei Liu, Jianlong Fu, Hongyang Chao, and Haibin Ling. Searching the search space of vision transformer. *Advances in Neural Information Processing Systems*, 34:8714–8726, 2021. 2, 5
- [8] Marius Cordts, Mohamed Omran, Sebastian Ramos, Timo Rehfeld, Markus Enzweiler, Rodrigo Benenson, Uwe Franke, Stefan Roth, and Bernt Schiele. The cityscapes dataset for semantic urban scene understanding. In *Proceedings of the IEEE conference on computer vision and pattern recognition*, pages 3213–3223, 2016. 2, 7, 11, 12
- [9] Xiaoyi Dong, Jianmin Bao, Dongdong Chen, Weiming Zhang, Nenghai Yu, Lu Yuan, Dong Chen, and Baining Guo. Cswin transformer: A general vision transformer backbone with cross-shaped windows. In *Proceedings of the IEEE/CVF Conference on Computer Vision and Pattern Recognition*, pages 12124–12134, 2022. 6, 7, 11, 14, 15
- [10] Alexey Dosovitskiy, Lucas Beyer, Alexander Kolesnikov, Dirk Weissenborn, Xiaohua Zhai, Thomas Unterthiner, Mostafa Dehghani, Matthias Minderer, Georg Heigold, Sylvain Gelly, et al. An image is worth 16x16 words: Transformers for image recognition at scale. In *International Conference on Learning Representations*, 2020. 1, 2
- [11] David Eigen, Christian Puhresch, and Rob Fergus. Depth map prediction from a single image using a multi-scale deep network. *Advances in neural information processing systems*, 27, 2014. 7
- [12] Yuan Gao, Haoping Bai, Zequn Jie, Jiayi Ma, Kui Jia, and Wei Liu. Mtl-nas: Task-agnostic neural architecture search towards general-purpose multi-task learning. In *Proceedings of the IEEE/CVF Conference on computer vision and pattern recognition*, pages 11543–11552, 2020. 2
- [13] Yuan Gao, Jiayi Ma, Mingbo Zhao, Wei Liu, and Alan L Yuille. Nddr-cnn: Layerwise feature fusing in multi-task cnns by neural discriminative dimensionality reduction. In *Proceedings of the IEEE/CVF conference on computer vision and pattern recognition*, pages 3205–3214, 2019. 2, 7
- [14] Pengsheng Guo, Chen-Yu Lee, and Daniel Ulbricht. Learning to branch for multi-task learning. In *International Conference on Machine Learning*, pages 3854–3863. PMLR, 2020. 3
- [15] Zichao Guo, Xiangyu Zhang, Haoyuan Mu, Wen Heng, Zechun Liu, Yichen Wei, and Jian Sun. Single path one-shot neural architecture search with uniform sampling. In *European conference on computer vision*, pages 544–560. Springer, 2020. 2, 3, 5
- [16] Eric Jang, Shixiang Gu, and Ben Poole. Categorical reparametrization with gumble-softmax. In *International Conference on Learning Representations (ICLR 2017)*. Open-Review. net, 2017. 5, 8
- [17] Yanghao Li, Chao-Yuan Wu, Haoqi Fan, Karttikeya Mangalam, Bo Xiong, Jitendra Malik, and Christoph Feichtenhofer. Mvitv2: Improved multiscale vision transformers for classification and detection. In *Proceedings of the IEEE/CVF Conference on Computer Vision and Pattern Recognition*, pages 4804–4814, 2022. 2, 6, 7, 11, 14, 15
- [18] Tsung-Yi Lin, Piotr Dollár, Ross Girshick, Kaiming He, Bharath Hariharan, and Serge Belongie. Feature pyramid networks for object detection. In *Proceedings of the IEEE conference on computer vision and pattern recognition*, pages 2117–2125, 2017. 4
- [19] Shikun Liu, Edward Johns, and Andrew J Davison. End-to-end multi-task learning with attention. In *Proceedings of the IEEE/CVF conference on computer vision and pattern recognition*, pages 1871–1880, 2019. 7, 11
- [20] Ze Liu, Yutong Lin, Yue Cao, Han Hu, Yixuan Wei, Zheng Zhang, Stephen Lin, and Baining Guo. Swin transformer: Hierarchical vision transformer using shifted windows. In *Proceedings of the IEEE/CVF International Conference on Computer Vision*, pages 10012–10022, 2021. 1, 2, 4, 6, 7, 11, 12, 14, 15
- [21] Jonathan Long, Evan Shelhamer, and Trevor Darrell. Fully convolutional networks for semantic segmentation. In *Proceedings of the IEEE conference on computer vision and pattern recognition*, pages 3431–3440, 2015. 6
- [22] Kevis-Kokitsi Maninis, Ilija Radosavovic, and Iasonas Kokkinos. Attentive single-tasking of multiple tasks. In *Proceedings of the IEEE/CVF Conference on Computer Vision and Pattern Recognition*, pages 1851–1860, 2019. 5, 6
- [23] Ishan Misra, Abhinav Shrivastava, Abhinav Gupta, and Martial Hebert. Cross-stitch networks for multi-task learning. In *Proceedings of the IEEE conference on computer vision and pattern recognition*, pages 3994–4003, 2016. 2, 7
- [24] Eslam Mohamed and Ahmad El Sallab. Spatio-temporal multi-task learning transformer for joint moving object detection and segmentation. In *2021 IEEE International Intelligent Transportation Systems Conference (ITSC)*, pages 1470–1475. IEEE, 2021. 1

- [25] Sebastian Ruder, Joachim Bingel, Isabelle Augenstein, and Anders Søgaard. Latent multi-task architecture learning. In *Proceedings of the AAAI Conference on Artificial Intelligence*, volume 33, pages 4822–4829, 2019. [2](#), [7](#)
- [26] Hongje Seong, Junhyuk Hyun, and Euntai Kim. Video multi-task transformer network. In *Proceedings of the IEEE/CVF International Conference on Computer Vision Workshops*, pages 0–0, 2019. [1](#)
- [27] Nathan Silberman, Derek Hoiem, Pushmeet Kohli, and Rob Fergus. Indoor segmentation and support inference from rgb-d images. In *European conference on computer vision*, pages 746–760. Springer, 2012. [2](#), [7](#), [11](#)
- [28] Trevor Standley, Amir Zamir, Dawn Chen, Leonidas Guibas, Jitendra Malik, and Silvio Savarese. Which tasks should be learned together in multi-task learning? In *International Conference on Machine Learning*, pages 9120–9132. PMLR, 2020. [3](#)
- [29] Ximeng Sun, Rameswar Panda, Rogerio Feris, and Kate Saenko. Adashare: Learning what to share for efficient deep multi-task learning. *Advances in Neural Information Processing Systems*, 33:8728–8740, 2020. [2](#), [3](#), [5](#), [6](#), [7](#), [8](#), [11](#)
- [30] Mingxing Tan and Quoc V Le. Efficientnet: Rethinking model scaling for convolutional neural networks. In *ICML*, 2019. [2](#)
- [31] Hugo Touvron, Matthieu Cord, Matthijs Douze, Francisco Massa, Alexandre Sablayrolles, and Hervé Jégou. Training data-efficient image transformers & distillation through attention. In *International Conference on Machine Learning*, pages 10347–10357. PMLR, 2021. [1](#)
- [32] Zhou Wang, Alan C Bovik, Hamid R Sheikh, and Eero P Simoncelli. Image quality assessment: from error visibility to structural similarity. *IEEE transactions on image processing*, 13(4):600–612, 2004. [6](#)
- [33] Enze Xie, Wenhai Wang, Zhiding Yu, Anima Anandkumar, Jose M Alvarez, and Ping Luo. Segformer: Simple and efficient design for semantic segmentation with transformers. *Advances in Neural Information Processing Systems*, 34:12077–12090, 2021. [4](#), [7](#), [8](#), [12](#)
- [34] Hanrong Ye and Dan Xu. Inverted pyramid multi-task transformer for dense scene understanding. In *Computer Vision—ECCV 2022: 17th European Conference, Tel Aviv, Israel, October 23–27, 2022, Proceedings, Part XXVII*, pages 514–530. Springer, 2022. [1](#)
- [35] Hanrong Ye and Dan Xu. Taskprompter: Spatial-channel multi-task prompting for dense scene understanding. In *The Eleventh International Conference on Learning Representations*, 2023. [1](#)
- [36] Jiahui Yu, Pengchong Jin, Hanxiao Liu, Gabriel Bender, Pieter-Jan Kindermans, Mingxing Tan, Thomas Huang, Xiaodan Song, Ruoming Pang, and Quoc Le. Bignas: Scaling up neural architecture search with big single-stage models. In *European Conference on Computer Vision*, pages 702–717. Springer, 2020. [2](#), [5](#), [11](#)
- [37] Amir R Zamir, Alexander Sax, William Shen, Leonidas J Guibas, Jitendra Malik, and Silvio Savarese. Taskonomy: Disentangling task transfer learning. In *Proceedings of the IEEE conference on computer vision and pattern recognition*, pages 3712–3722, 2018. [1](#), [2](#), [3](#), [6](#), [7](#), [11](#), [12](#)
- [38] Lijun Zhang, Xiao Liu, and Hui Guan. Automtl: A programming framework for automating efficient multi-task learning, 2021. [2](#), [6](#), [7](#), [11](#)
- [39] Hengshuang Zhao, Jianping Shi, Xiaojuan Qi, Xiaogang Wang, and Jiaya Jia. Pyramid scene parsing network. In *Proceedings of the IEEE conference on computer vision and pattern recognition*, pages 2881–2890, 2017. [8](#)

A. Pseudo-code of Multi-task NAS Pipeline

Algorithm 1 Multi-task NAS pipeline.

Notations:

- T**: all training tasks
- D**: all training data
- \mathcal{A} : supernet with skeleton space **S** and the weight W .
- a : subnet sampled from \mathcal{A} with weights from W .

Multi-task Supernet Train

- 1: **for** $_$ **in** range(epochs) **do**
- 2: **for** $x, y(\mathbf{T})$ **in** **D** **do**
- 3: $a \leftarrow \text{RANDOMSAMPLE}(\mathcal{A})$
- 4: Calculate l according to Eqn.(5)
- 5: Update \mathbf{U}' and W by l .
- 6: **end for**
- 7: **end for**

Skeleton Space Search

- 1: Get discrete \mathbf{U} from \mathbf{U}' by column-wise argmax .
- 2: Get $|\mathbf{T}|$ task-favored skeletons $s_1, s_2, \dots, s_{|\mathbf{T}|}$ by \mathbf{U} .
- 3: Union skeletons to find the smallest skeleton \hat{s} where every $s_i \subseteq \hat{s}$

Cell Space Search

- 1: Search cell hyper-parameters for skeleton \hat{s} according to Eqn.(7).
-

B. Datasets and Implementation Details

B.1. 16 tasks learning on Taskonomy

Taskonomy [37] consists of 4.5 million images from 500 buildings with annotations available for 26 tasks. Considering the huge size of full dataset, we use the official tiny split from it, which consists of 260K images from 25 buildings for train, 60K images for validation, and 54K images for test. Unlike previous methods [29, 38] that only evaluate 5 dense prediction tasks, we include 11 more tasks from the original 26 tasks that covers more varieties of task types like classification, point regression, and unsupervised metric learning. Due to the huge capacity of this dataset, we directly resize all the input images to 224×224 to train and test all vision transformers without any data augmentation. We follow the same loss criterion as in the original Taskonomy for all vision transformers.

For Taskonomy [37], we train AutoTaskFormer as well as the other baseline vision transformers for 30 epochs. We adopt the sandwich rules [36] that sample the largest, the smallest, and two middle sized subnets to train the supernet like AutoTaskFormer and AutoFormer [6] to aggregate their gradients in each iteration. We use AdamW optimization with a base learning rate of $5e-4$ for batch size of 64. We use a linear warm-up strategy in the first epoch and a cosine scheduler to decrease learning rate to $5e-6$. We set the weight

Models		#Params (M)	#FLOPs (G)	Δ_T
Swin [20]	Tiny	48.5	13.4	4.7
	Small	69.8	17.6	5.4
	Base	107.7	24.2	5.7
Cswin [9]	Tiny	31.3	8.1	3.3
	Small	43.7	10.5	3.7
	Base	97.6	23.4	3.9
MViTv2 [17]	Tiny	44.3	11.6	5.9
	Small	55.0	16.1	5.6
	Base	71.5	18.0	6.7
AutoTaskFormer Auto		22.3~108.7	6.2~24.7	7.0~9.4

Table 6. FLOPs of different vision transformers on Taskonomy.

decay to 0.05 for regularization. In Tab. 7, we provide task loss weights λ_k and the baseline single-task learning benchmark to calculate the multi-task relative performance. We report the FLOPs of different multi-task vision transformers in Tab. 6.

B.2. 2 tasks learning on Cityscapes

Cityscapes [8] consists 5K high-resolution street-view images. We adopt 19-class annotation for semantic segmentation and estimate depth following [19]. All images are resized to 256×256 by random flipping and cropping during training, and are resized to 256×512 during test. We train AutoTaskFormer as well as the other baseline vision transformers for 200 epochs. We use AdamW optimization with a base learning rate of $5e-4$ for batch size of 8. We use cosine scheduler to decrease learning rate to $5e-6$ and set the weight decay to 0.05 for regularization. The task loss weights λ_k during training are set to 1 for both semantic segmentation and depth estimation.

We visualize both the single-scale and multi-scale skeletons and their multi-task architectures in Fig. 9. It indicates AutoTaskFormer shares the certain stage of knowledge between tasks and owns the individual knowledge for a single task.

B.3. 3 tasks learning on NYUv2

NYUv2 [27] consists of 1449 images from 464 different indoor scenes. We follow [19] to use 40-class semantic segmentation, depth estimation, and surface normal predictions in a 3 task scenario. We perform transfer learning on 3 tasks NYUv2 for 50 epochs. During training, we resize the input images to 224×224 by randomly cropping and test on the 224×224 center cropped images. We use AdamW optimization with a base learning rate of $5e-4$ for batch size of 8 and cosine scheduler to decrease learning rate to $5e-6$. The task weight losses λ_k for semantic segmentation, depth estimation, surface normal predictions are set to 1, 3, 20 respectively.

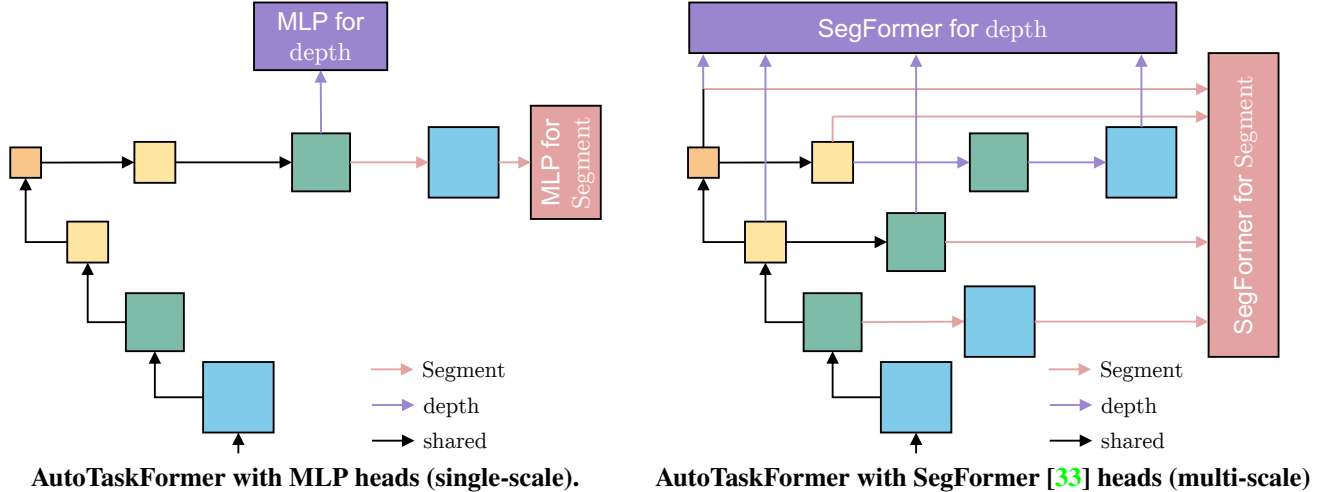


Figure 9. We visualized both the searched single-scale (Left) and multi-scale (Right) skeletons and their multi-task architectures for 2-tasks learning on **Cityscapes**.

	Point predictions			Dense predictions													
	Acc. \uparrow		loss \downarrow	mIoU \uparrow	MS-SSIM \uparrow											loss \downarrow	
	Obj.	Scene	Van. Pt.		SegSem	De	Dz	E2d	E3d	K2d	K3d	N	PC	R	AE	Seg2d	Seg2.5d
Swin-T (single-task)	47.9	60.3	1.567	31.0	86.6	86.6	94.5	73.0	96.6	56.4	75.7	67.3	68.7	96.0	0.446	0.150	
task loss weight (λ_k)	2	2	5	5	2	2	30	10	30	10	20	0.5	20	0.1	1	1	

Table 7. Results of single task baseline (Swin-T [20]) to train each task on Taskonomy. We provide the task weightings λ_k for 16 tasks.

#Param	Stride	Embed dim	Head Num	Depth	MLP ratio	Window
22.3 ~62.2M	1/4	{64, 96, 128}	{2, 3, 4}	{2, 4}	{3.5, 4}	{5, 7, 9}
	1/8	{160, 192, 224}	{5, 6, 7}			
	1/16	{352, 384, 416}	{11, 12, 13}			
	1/32	{732, 768, 800}	{23, 24, 25}			
37.2 ~108.7M	1/4	{96, 128, 160}	{3, 4, 5}	{2, 4}	{3.5, 4}	{5, 7, 9}
	1/8	{192, 256, 320}	{6, 8, 10}			
	1/16	{448, 512, 576}	{14, 16, 18}			
	1/32	{960, 1024, 1088}	{30, 32, 34}			

Table 8. The cell search space of AutoTaskFormer. For example, for AutoTaskFormer of size 22.3~62.2M, we search embedding dimension from the set {64, 96, 128}. **Note:** The embedding dim and number of heads are set according to the stride of cells while the others are irrelevant to the stride.

B.4. Detailed Cell Search Space

According to the constraints on model parameters, we partition the cell space following the designs of Swin-S and Swin-B. The detailed design is presented in Tab. 8.

B.5. Evolutionary Search

We search for subnets $\alpha \in \mathcal{A}$ according to $\gamma(\alpha)$ that yield the best multi-task performance under different resource constraints via the evolution search. Specifically, we first pick 50 random subnets in the cell space as seeds and set the

number of generations to 20. The top 10 subnets are picked as parents to generate the next generation by mutation and crossover. For a crossover, two randomly selected candidates are picked and crossed to generate a new one. For mutation, we first mutate depth and embedding dimension in each transformer layer with a probability of 0.4, and then mutate cell parameters in each block with a probability of 0.2 to produce new architecture.

C. Supplementary Comparing Results

We demonstrate that different tasks prefer different model complexities according to their favored skeletons. Thus, it is flexible to search smaller vision transformers for simple tasks. We supplement Fig. 6 with the other 14 tasks' performances in Fig. 10 to show that once trained AutoTaskFormer can provide different vision transformers for various tasks under various resource constraints.

D. Qualitative Results

We qualitatively compare the results of our AutoTaskFormer with other handcrafted vision transformer baselines. Fig. 11 shows the performance of 16 tasks learning on Taskonomy [37]. Fig. 12 shows the results of 2 tasks learning on cityscapes [8] with SegFormer [33] task heads.

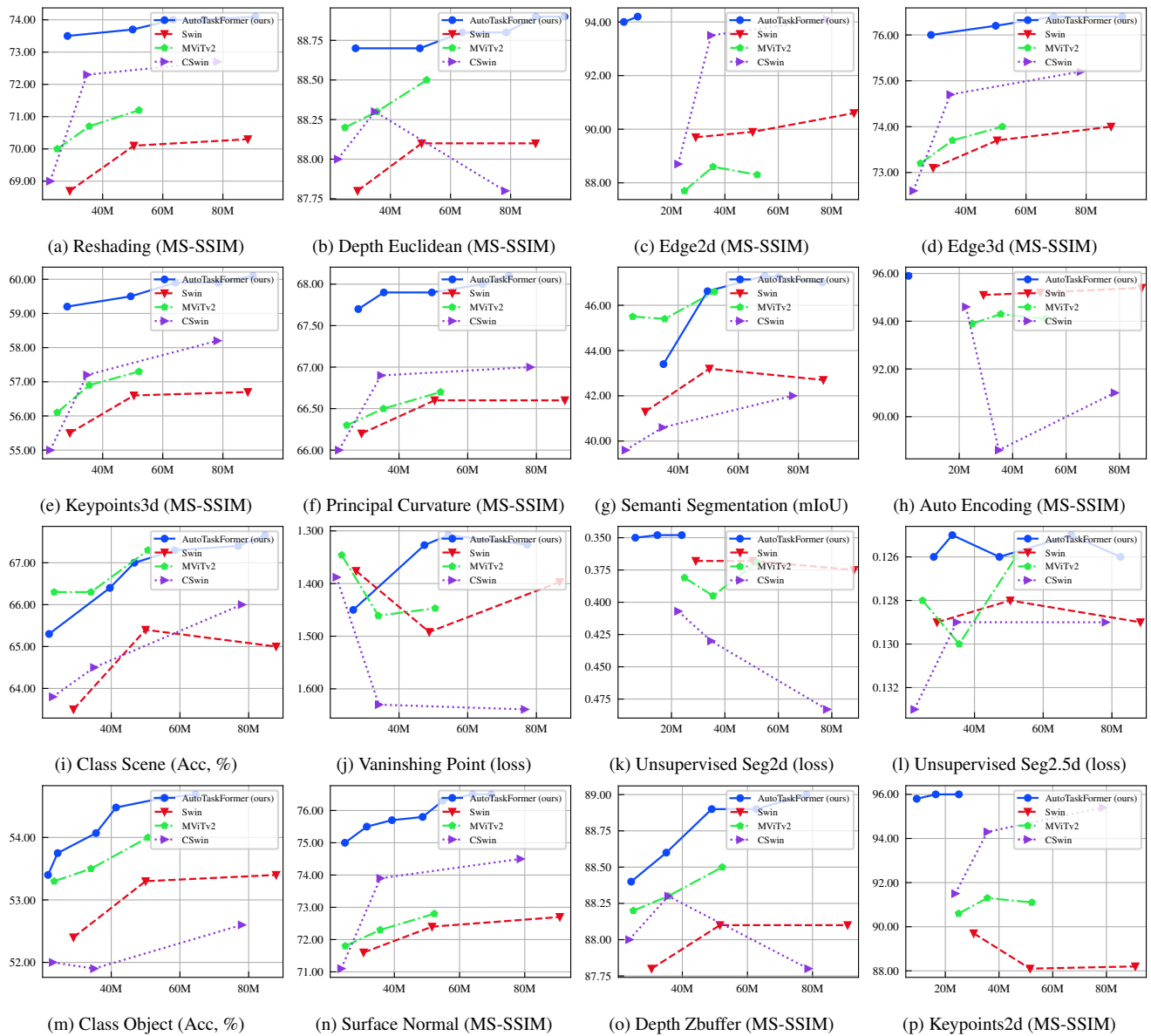


Figure 10. The performances of single-task vision transformers after 16 tasks training on Taskonomy. We compare AutoTaskFormer with other handcrafted vision transformers on all 16 tasks.

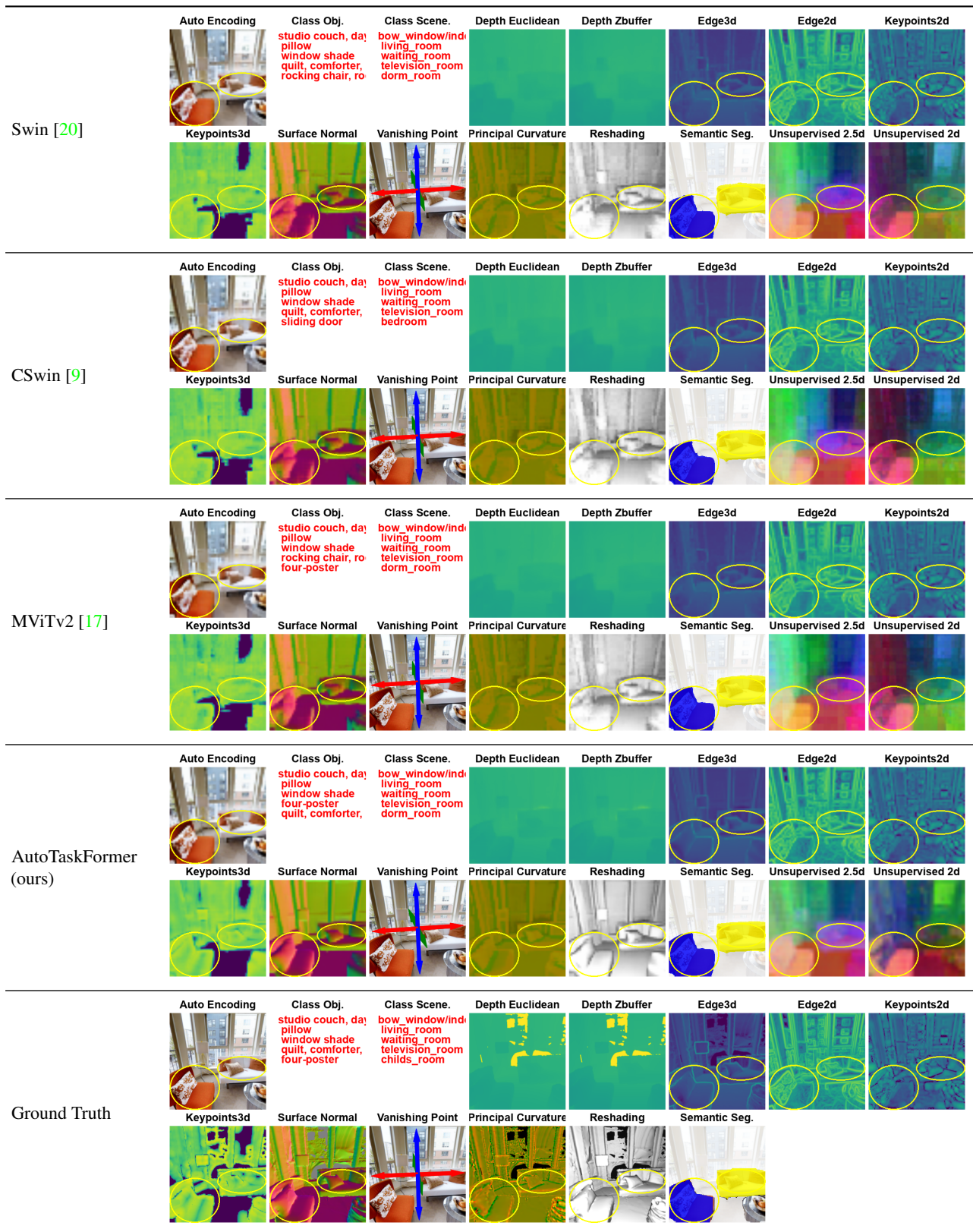


Figure 11. **Qualitative comparison for 16 tasks learning on Taskonomy (~40M parameters).** Our AutoTaskFormer outperforms other handcrafted multi-task vision transformers. Best seen on screen and zoomed within the yellow circled regions.

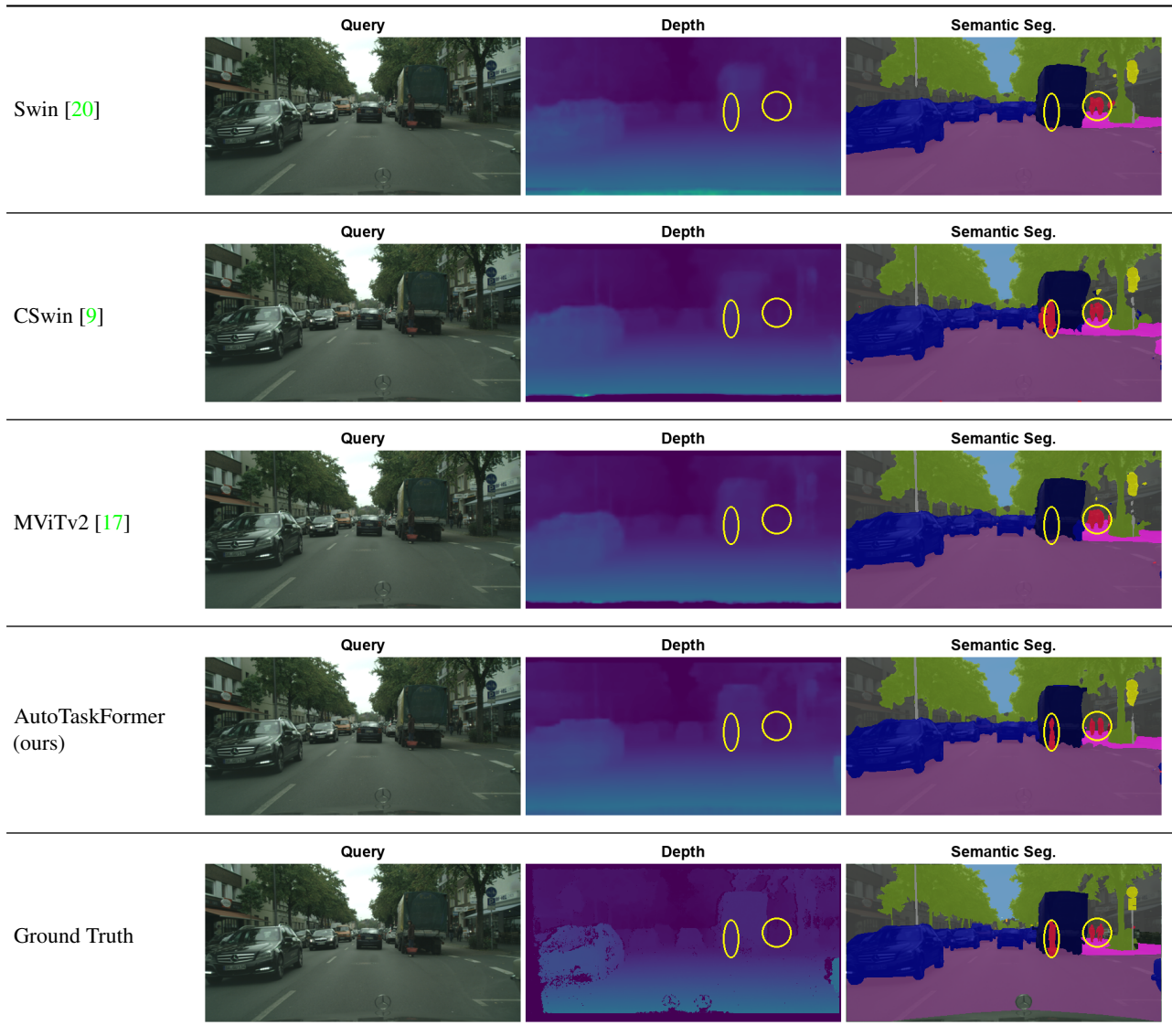


Figure 12. **Qualitative comparison for 2 tasks learning on Cityscapes (~30M parameters).** Our AutoTaskFormer outperforms other handcrafted multi-task vision transformers. Best seen on screen and zoomed within the yellow circled regions.